Melissa Kacena ORCID iD: 0000-0001-7293-0088

Christopher Collier ORCID iD: 0000-0003-2639-4290

Methodology, Selection, and Integration of Fracture Healing Assessments in Mice

Running title: Fracture Healing Assessments in Mice

Adam M. Knox[1], Anthony C. McGuire[1], Roman M. Natoli[1], Melissa A. Kacena[1,2], and Christopher D. Collier[1]

[1]Department of Orthopaedic Surgery, Indiana University School of Medicine, IN, USA

[2]Richard L. Roudebush VA Medical Center, IN, USA

*Corresponding Author:

Christopher D. Collier, MD

Department of Orthopaedic Surgery

Indiana University School of Medicine

1130 W Michigan Street, Fesler Hall 115

Indianapolis, IN, 46202, USA

ccollie@iu.edu

Authors' contributions

A.M. Knox: writing original draft, approval of submitted version

A.C. McGuire: writing original draft, approval of submitted version

R.M. Natoli: conceptualization, critical revisal, approval of submitted version

M.A. Kacena: conceptualization, critical revisal, approval of submitted version

This is the author's manuscript of the article published in final edited form as:

Knox, A. M., McGuire, A. C., Natoli, R. M., Kacena, M. A., & Collier, C. D. (2021). Methodology, Selection, and Integration of Fracture Healing Assessments in Mice. Journal of Orthopaedic Research, 39(11), 2295-2309. https://doi.org/10.1002/jor.25172

C.D. Collier: conceptualization, critical revisal, approval of submitted version

All authors have read and approved the final submitted manuscript.

Abstract

Long bone fractures are one of the most common and costly medical conditions encountered after trauma. Characterization of the biology of fracture healing and development of potential medical interventions generally involves animal models of fracture healing using varying genetic or treatment groups, then analyzing relative repair success via the synthesis of diverse assessment methodologies. Murine models are some of the most widely used given their low cost, wide variety of genetic variants, and rapid breeding and maturation. This review addresses key concerns regarding fracture repair investigations in mice and may serve as a guide in conducting and interpreting such studies. Specifically, this review details the procedures, highlights relevant parameters, and discusses special considerations for the selection and integration of the major modalities used for quantifying fracture repair in such studies, including: X-ray, micro-computed tomography, histomorphometric, biomechanical, gene expression and biomarker analyses.

Key Words: Fracture Healing, Mouse Models, X-ray, mRUST, micro-computed tomography, histology, biomechanics, preclinical

Background

In the United States, there were an estimated 2 million osteoporosis-related fractures with an associated total cost of $17 billion in 2005 (1). By 2025, these numbers are expected

to surpass 3 million osteoporotic fractures with anticipated total costs over $25 billion annually (2, 3). Contributing to this total economic burden are costs associated with lost productivity due to long recovery periods. For instance, an expected recovery from a closed tibial fracture with intramedullary stabilization is 3 to 6 months. This duration is often even longer in the 5-33% of fractures in the United States that result in delayed or non-union (4, 5). Studies investigating the mechanisms underlying repair and evaluating potential interventions are pivotal to expediting and improving fracture healing outcomes.

Endochondral ossification is essential to long bone fracture healing. The first stage of this process is hematoma formation, at which point ruptured vessels release immune cells and nutrients, and granulation and fibrous tissue begins to form. In this stage, hypoxic and biomechanical strain attenuates osteoblast differentiation in the fracture gap and promotes differentiation of chondrocytes leading to the second stage of healing, fibrocartilaginous callus formation. These cells proliferate and secrete a cartilaginous matrix serving as an early scaffold for further repair. As the callus matures, chondrocytes undergo apoptosis or trans-differentiate into osteoblasts (6-8). Concurrently, neovascularization proceeds at the cartilage-bone transition providing oxygen so that osteoblasts may generate mineralized bone, leading to the third stage of healing, bony callus formation. Once mineralized bone bridges the fracture gap, the final and longest stage of repair begins, bone remodeling. At this point, osteoclasts degrade recently generated bone at the fracture site to allow for revisions of physiological contour and structure (6, 9, 10). As endochondral ossification occurs immediately adjacent to the fracture line, intramembranous ossification may proceed subperiosteally, producing a hard callus which supports rigidity (6, 11).

There are several factors believed to influence the structure and composition of the final product of fracture repair. For instance, there is a perceived correlation between the amount of cartilage that forms and the interfragmentary motion during repair, with abundant motion resulting in higher cartilage content and vice versa. Due to this phenomena, the choice of fixators in mice studies may have a profound impact on fracture callus composition (12). This entire process generally occurs within 3 to 6 months in humans and 5 weeks in mice, and occurs via similar mechanisms between species (13). It is important to keep this paradigm of fracture healing in mind when considering the various modalities used to study fracture healing to understand what each modality may provide depending on time post-injury.

Animal models are frequently used in order to adequately monitor and characterize this healing process, as they are one of the most effective simulations of *in vivo* bone healing available. These studies allow precise fractures to be created without the numerous confounding variables present in human fracture studies. Bones may also be obtained from humanely euthanized animal subjects at various stages of the healing process to measure the outcomes of healing bone. Of animals, mice are particularly useful as they mature quickly, are inexpensive to breed and maintain high populations, and have many genetic variants and molecular probes readily available (14). A variety of fracture models have been proposed in mice, including fractures created by closed three-point bending, impact loading, or open surgical approaches (15, 16).

In order to characterize underlying mechanisms, identify deterministic factors, and develop interventions to expedite and improve fracture healing outcomes, diverse sets of

fracture repair assessments must be tactfully selected and synthesized. This review details the procedures, highlights relevant parameters, and discusses special considerations for the selection, integration, and planning of the major modalities of quantifying fracture repair, including: X-ray, micro-computed tomography (μCT), histomorphometric, biomechanical, gene expression and biomarker analyses.

Radiographs

Radiographic evaluation of fractures involves taking X-rays throughout the course of fracture repair and may offer a non-invasive approximation of fracture repair progress and success (Figure 1). Traditionally, they have not often been used to generate numerical data, however this may change following validation of new scoring systems such as the standard and modified radiographic union scale in tibia (RUST and mRUST, respectively).

Procedure

These evaluations are the least invasive and time intensive, and therefore are generally performed immediately following fracture induction, periodically throughout the repair process, and prior to euthanasia. For RUST/mRUST scoring, two orthogonal or perpendicular views should be obtained for each time point. Mice need to be anesthetized for the duration of X-ray collection to minimize motion artifact, which may require specialized radiography systems.

For X-ray scoring methods such as RUST/mRUST, at least two or three blinded reviewers is preferred to generate scores (17-19). Training of the scorers in advance may

also be necessary, as orthopedic surgeons who use RUST/mRUST scores in human clinical practice may need time to acclimate to murine models.

Outcomes

Traditional

Traditionally, X-rays in fracture studies serve to display the progression of fracture healing, with minimal attempts to generate numerical data. Corrales *et al*. (20) found that the most commonly evaluated X-ray criteria in animal studies were bridging of fracture by callus, bone or trabeculae; bridging of the fracture at three or more cortices; and obliteration of the fracture line and/or cortical continuity. However, these were not deemed reliable measures due to high intra and inter-class variability (20). Other studies have found that callus size, measured from radiographs, correlates with μCT measures such as cross-sectional area and bone mineral density (BMD) (21, 22), while radiographically determined cortical continuity seems to be an accurate indicator of mechanical strength (23). Promising new approaches to quantifying X-ray are RUST and mRUST (Table 1).

RUST and mRUST

The RUST scoring system, first developed by Whelan *et al*. (24), was designed to reproducibly grade tibia fracture healing in humans. RUST scoring is judged from orthogonal radiographic images of the tibial fracture site, with each cortex being graded from 1-3 then summing all cortices for a total between 4 (no healing) and 12 (completely healed) (Table 1) (24). Previous radiographic scoring methods, such as those proposed by

Hammer *et al*., predicted healed fractures at a relatively low rate of 50%, with an interclass correlation coefficient (ICC) of 60%. RUST has been found to have significantly higher ICCs of 70% reported by Litrenta *et al*. (25) and 86% by Kooistra *et al*. (18). RUST scoring also has the benefit of being relatively simple, asking the assessor to only comment on the presence or absence of a fracture line or callus, as opposed to the Hammer scale, which asked assessors to rate the degree of fracture line and the size of callus.

Modified RUST scoring, or mRUST, is an altered RUST score model that asks assessors to judge if a callus is present, bridging, or remodeled rather than only if it is present or absent. As such, the mRUST score ranges from 1-4 for each cortex rather than 1-3, with total values between 4 and 16 (Table 1). mRUST scoring has demonstrated higher ICC than RUST scoring (17). Both of these scoring methods have been validated in human tibial fractures, but evidence supporting use in animal femur fracture models is present (17, 25).

In murine fracture studies, evidence supporting the implementation of RUST and mRUST is limited but promising. Cooke *et al*. found both RUST and mRUST to have an excellent relationship to structural and biomechanical metrics (19). Both positively correlate with BMD, bone volume / tissue volume (BV/TV), callus strength, and callus rigidity, with mRUST generally having slightly higher correlation coefficients, with an ICC of 0.71 in mRUST and an ICC of 0.63 in RUST. Additionally, 90% of scorers agreed that scans with mRUST scores of 13 were “healed”, and 100% agreed that scans with mRUST scores of 8 were “not healed” (19).

Biomarkers

Biomarkers offer noninvasive, inexpensive means of assessing fracture healing stage and underlying processes and have shown potential as independent predictors of fracture healing success. Selected biomarkers are generally serum peptides that represent either systemic or local processes facilitating fracture repair, or extracellular matrix components that are produced or degraded during repair (26).

Procedure

Serum biomarkers are quantified using a variety of immunoassay techniques. Investigations begin with serum collection targeted to specific stages of repair or periodically throughout a study. Serum is then assessed, often with a form of enzyme-linked immunoassay (ELISA) such as sandwich assays, competitive assays, and antigen down assays. Sandwich assays involve using two antibodies that bind different sites on an antigen or ligand of the molecule of interest. The first antibody, the capture antibody, binds the molecule of interest with high specificity and agglutinates it to the assay tray. The second antibody binds at a separate site on the molecule of interest, and is conjugated to a reporter molecule, often an enzyme that catalyzes a visualizable reaction or possesses innate fluorescence. Depending on what is conjugated to the detection antibody, spectrophotometric, fluorescence, or chemiluminescence readers are employed to detect a signal proportionate to the amount of target antigen present in the sample. From these measures, serum concentration of the molecule of interest may be determined. Sandwich assays tend to be sensitive and robust and are of the most commonly used, however assay

format will likely depend on what reagents are available and the dynamic range required for the assay (27).

Outcomes

Hussein *et al* reports 50 serum proteins of interest that exhibit predictable trends throughout fracture repair (28). Examples of these markers, often reported in fracture repair studies, include TRAP, RANKL and CTX reflecting osteoclast activity, ALP, PNP and OC reflecting osteoblast activity, CXM and collagen X reflecting chondrocyte activity and TGF-B, TNF-a, and VEGF reflecting immune activity and angiogenesis (29-32).

Assessment of these biomarkers may elucidate how underlying fracture repair processes are altered in various circumstances, manifesting in distinct repair outcomes (29-32). Furthermore, recent reviews have investigated the potential of these biomarkers to serve as independent predictors of fracture repair success (33-35). This is of particular interest as reliable correlations could enable earlier clinical identification of non-union, improving clinical outcomes.

Micro-Computed Tomography

Micro-computed tomography (μCT) involves taking a series of X-ray images of the sample at different rotations, and then using computer algorithms to reconstruct a 3D image stack for analysis. This reconstruction enables high resolution visualization of fracture callus architecture. These assessments are generally performed *ex vivo* for the

quantification of mineralized bone, however, may be adapted for *in vivo* and/or soft tissue analysis (e.g. cartilage, vasculature).

Procedure

Sample Preparation

Ex vivo sample preparation for μCT often depends on subsequent testing planned for each sample, although each sample within a set for μCT should be fixed in the same manner. For instance, sets to undergo later mechanical testing should not be fixed, as this can alter structural properties of bone (36). Freezing in sterile phosphate buffered saline (PBS) is a less deleterious form of storage for samples destined for mechanical testing (37). Sets to undergo other assessments (e.g. histological staining) may be fixed, usually using formalin or organic solvents such as alcohols or acetone. Prior to scanning, bones are cleaned of surrounding tissue and are generally placed in a holder filled with a medium such as saline or ethanol and wrapped in low-density foam or gauze to limit desiccation and motion artifact.

μCT may also be conducted *in vivo* with additional considerations such as animal placement, anesthesia, and image registration (38). *In vivo* μCT is advantageous for its ability to generate longitudinal data without requiring mouse sacrifice. However, its resolution is limited by anesthetic time and the negative effects of radiation exposure may disrupt bone homeostasis and fracture repair (39, 40).

Acquiring projection images

Image quality and scan times are dependent on a number of adjustable parameters including X-ray tube voltage, intensity, rotation step, integration time, and voxel size (41). There is not great consensus among murine fracture studies on ideal values for these settings. General ranges for these values in such studies are voltage (50-80kV), intensity (80-200μA), rotation step (0.2-0.7º), integration time (250-1500ms), and voxel size (5-20μm) (15, 21, 42-45). Large deviations from these ranges may distort derived measures. For instance, when the voxel size is too large there may be overestimation of material size/density, but when it is too small there may be excessive noise (46).

During scans, samples are generally aligned with the long axis of the scanner, aluminum or copper filters may be placed in the beam path to reduce beam hardening, and pixel binning may be used to improve contrast at the cost of reduced resolution (41).

Computerized reconstruction and processing

After scanning, 3D image stacks are reconstructed from the produced rotation image projections, using software such as NRecon or image processing language (IPL) and processed. Processing primarily involves selecting the volume of interest (VOI), voxel thresholding and applying filters.

Generally, in fracture studies, the VOI is the fracture callus. This region may be selected as the volume within an absolute length or fraction of total bone length above and below the fracture line center, or by manually tracing the proximal and distal boundaries using semi-automated segmentation tools. The cortex and intramedullary canal are usually

excluded from the final VOI, although may be included in studies using μCT to quantify fracture bridging (Figure 2) (15, 21, 42-45).

Once the VOI has been identified, threshold values are selected to differentiate tissue types within based on voxel intensity. A single threshold may be selected if the desire is only to delineate between bone and non-bone, however additional thresholds may be necessary if, for instance, bone must also be distinguished from a scaffold or implanted device, or differentiation between various degrees of mineralization is desired. Thresholds are generally either carefully selected absolute values or percentages of maximum grey value (Figure 3) (15, 21, 41-45).

Lastly, filters may be carefully implemented in order to minimize noise without blurring images, and to correct potential ring artifacts and beam hardening (41).

Outcomes

μCT parameters pertinent to fracture healing include tissue volume (TV), tissue mineral density (TMD), bone volume (BV), bone volume fraction (BV/TV), bone mineral density (BMD) and the polar moment of inertia (pMOI) (Table 2). TV, TMD, BV/TV, and BMD measure the volume or fractional volume of mineralized and non-mineralized tissues as well as their respective hydroxyapatite densities. pMOI, is the resistance of an object to change in rotational velocity based solely on its geometry. Briefly stated, the more area an object possesses in a certain cross section, and the further displaced that area is from the center of the rotational axis, the more resistant it is to changes in rotational velocity (including bending and torsion) at that cross section (47).

Each of these measures has been found to show aberrancy following fracture and resolution throughout repair, as well as correlation to biomechanical values. pMOI, BV, and BMD tend to correlate most with biomechanical properties, while TV and TMD tend to show the most consistent convergence to non-fractured values throughout repair (21, 44, 45).

Murine fracture studies less consistently include µCT measures of trabecular microstructure such as trabecular separation (Tb.Sp,) trabecular thickness (Tb.Th), and trabecular number (Tb.N). Data analyzing trabecular microstructure throughout fracture repair in mice is limited but appears to follow predictable trends throughout the progression of endochondral ossification in mice. Recent studies have found trabecular number and thickness to increase most drastically in the first 1-3 weeks post fracture, as cartilage is converted to woven, trabecular and cortical bone, with apparent tapering to still greater than pre-fracture values by week 5, as bone is resorbed and remodeled (48-51). Trends in trabecular separation exhibit roughly inversely proportional changes (48-50). These values have also been found to correlate with mechanical functionality throughout repair (50). Imaging the wide range of trabecular mineralization during repair may require smaller voxel sizes and more imaging time (52). Additionally, with the use of contrast, µCT may also be utilized to assess soft tissues such as cartilage and vascularization (53, 54).

Histomorphometry

Histological staining followed by histomorphometry offers another avenue for assessment of the fracture callus that is best for differentiating between tissue types

(cartilage, fibrous, bone, marrow). It may only be performed *ex vivo* and is destructive of samples. These assessments involve staining thin sections with a variety of dyes, many of which selectively color certain structures and tissue types, allowing for straightforward identification and computer analysis. Data gathered from these analyses may include the area or relative percentage of area consisting of cartilage, bone, fibrous tissue, or marrow.

Procedure

Slide preparation

Histologic analysis begins with removing the bone to be analyzed from the humanely euthanized mouse. The sample is then fixed in formalin or a high percentage ethanol solution to halt proteolytic enzymes and bacterial proliferation, then it is dehydrated by further increasing the ethanol percentage to drive out excess water. It should be noted that while formalin (typically 10% neutral buffered formalin and 4% paraformaldehyde) is simple, fast, and easily available, it does decrease the biomechanical strength of bone over time, degrades nucleic acids, and is both toxic and carcinogenic (55, 56). One alternative is glyoxal, which provides similar aldehyde-based fixation with less toxicity (56, 57). Some patented glyoxal-based formulas, such as HistoChoice, have been shown to improve staining of bone tissue samples using stains such as Toluidine blue, Von Kossa, and alkaline phosphatase staining (58). For typical histologic sectioning, bones are decalcified in EDTA or another decalcifying agent, and then embedded in paraffin, or are embedded into poly(methyl methacrylate) if preservation of calcified/mineralized bone is desired. EDTA is typically the agent of choice as it preserves the antigenicity of the sample for immunohistochemical staining. However, EDTA requires a long incubation

period (around 21 days), so more rapid acting agents such as nitric acid or formic acid may be used if time is limited, as these agents work more rapidly (around 8 days). This rapid action, however, decreases the preservation and staining of IHC markers (59). A study utilizing fluorescence marking may wish to avoid paraffin embedding as it may disrupt the desired fluorescent emission (60). In this case, samples may be prepared using cryoembedding and cyrosectioning, in which samples are frozen in a solution such as Optimal Cutting Temperature (O.C.T.) compound, a mixture of glycols and resins, in order to maintain fluorescence after sectioning (60). Blocks containing embedded tissues are then sliced into micrometer wide sections and stained before analysis.

Staining

Structural histomorphometric staining protocols are selected in order to consistently distinguish cartilage, bone, and fibrous tissue, for quantification with semi-automated measurement techniques. The most frequently used staining method is a hematoxylin and eosin stain, which stains based on the acidophilic or basophilic properties of the tissue. Also available are alcian blue and picrosirius red, which stains proteoglycan and collagen, respectively (Figure 4). There are many other stains for bone tissues such as Von Kossa, Gömöri trichrome, etc., safranin O for cartilage, and endomucin for angiogenesis (61). A list of common stains and their uses is shown in Table 3. After staining, slides are assessed using semi-automated techniques such as open-source GNU Image Manipulation Program (www.gimp.org). This free select tool can be used to demarcate each stained area to generate associated pixel counts, which are then converted

to um^2 using a standard scale. Other available tools include Adobe Photoshop and ImageJ (62).

Certain studies may also conduct immunohistochemistry (IHC), which involves using antibodies linked to fluorescent or otherwise identifiable proteins that bind specific molecular markers of repair processes, enabling quantification of their temporal and spatial presence, absence or relative abundance (9, 10, 60). These techniques generally utilize antibodies conjugated to enzymes that catalyze detectable reactions, for the visualization and localization of targeted molecules (63). Common IHC stains for bone are included in Table 3.

Outcomes

Histomorphometric parameters typically used for fracture repair outcomes include: the total or fractional areas of osseous, cartilage, and fibrous tissue, as well as the total callus area and void area (Table 2). These values have been shown to correlate with other methods of assessment throughout fracture repair and indicate key stages of fracture healing. Histologic measures of callus size, diameter, and area – independent of tissue composition – can be used to predict or corroborate biomechanical properties, including strength, stiffness, and moments of inertia (64-66). Histologic measures of mineralized tissue in callus are highly correlated with μCT outcomes of BMD, BV/TV, and mechanical stiffness (64, 67), and increased presence of cartilaginous or fibrous tissue within the fracture defect has been linked to increased incidence of union and non-union respectively (68).

Immunohistochemistry measures may be included in order to further elucidate the underlying molecular processes which manifest in repair outcomes, as well as observe early stages of bone healing, such as hematoma and chondrogenesis, as μCT and X-ray would fail to detect this non-mineralized tissue (16, 69, 70).

Biomechanics

Biomechanical testing offers the most direct quantification of bone's ability to support efficient locomotion and is thus pivotal for determining the functionality of the end product of fracture repair. These tests involve applying force, chiefly through bending or torsion, while tracking displacement until material failure occurs. Simultaneous recording of force and displacement produces a curve from which numerous mechanical properties can be derived.

Procedures

Bending

Mechanical testing is most commonly conducted by bending, of which there are two main varieties: 3 point and 4 point. In both 3 and 4 point bending, the bone is set on two supports separated by just less than the sample length. In 3-point bending, a steadily increasing downward force is then applied at the center of the two supports until fracture occurs (Figure 5A). With 4-point bending, the procedure is similarly conducted, except two downward forces are applied each equidistant from the center of the bone (Figure 5B). The theoretical advantage to 4-point bending is that it more uniformly spreads the moment of bending between the two points of force application to account for callus

heterogeneity. However, in practice, it is difficult to position most bones so both prongs make equal contact, so it has not been used as often as 3-point bending (47, 71).

Torsion

Torsion tests are performed less frequently than bending tests; however, they are preferred, especially for fracture studies, as they best account for bone heterogeneity by distributing the force most equally throughout the entire sample and are less prone to experimental variation (72). For these tests, samples are first fixed on both ends into circular or rectangular grips of the testing device. Then one end is twisted while the other is held firmly, or both ends are twisted in opposite directions producing torsional stress until material failure (Figure 5C). The amount of torque required to complete each incremental turn (usually of about half a degree) is recorded, and this data is used to generate a torque-angular displacement curve similar to that of the bending tests (47, 71).

Outcomes

Primary measures of torsional tests include ultimate torque, torsional stiffness, twist to fail, and toughness (Table 2). Ultimate torque is the torque at which material failure occurs. Torsional stiffness is the torque required to make each individual rotation (the slope of the force-displacement relationship) prior to the yield point (the point of delinearization of the force-displacement relationship where small increments of force provoke large displacements of bone due to compounding micro cracks decreasing stiffness). Twist to fail is the degrees of rotation completed to produce fracture, and

toughness is the total energy to fracture (area under the curve of force-displacement relationship) (Figure 6).

Primary measures of bending tests are derived from a force-displacement relationship rather than a torque-angular displacement relationship but are otherwise conceptually similar and include maximum force, stiffness, and toughness (Table 2).

Differences in fracture repair stage and/or success may manifest in key failure patterns on biomechanical testing. For instance, fracture calluses with a higher portion of cartilage or granulation tissue tend to withstand higher interfragmentary strain (change in fracture gap width divided by original fracture gap width) before failure, and rupture with a more ductile pattern (ultimate stress greater than fracture stress) compared to calluses with a higher portion of mature bone. Specifically, fully bridged calluses tend to rupture under strains of <2%, cartilaginous calluses under strains of 2-10%, and granulation tissue or non-unions under strains of up to 100% (12, 73). Furthermore, specific modes of bone failure, such as at the bone-graft interface in critical size defect repairs, often have characteristic patterns on biomechanical testing (74).

Gene Expression

Genetic approaches aim to elucidate the intricate cellular and molecular processes underlying fracture repair and are often included to explain other structural, compositional, and mechanical outcomes or to test specific hypotheses. Among fracture repair investigations, genetic approaches encompass a particularly wide breadth of possibilities. Two common techniques are using reporter mice and performing gene

expression analyses. A summary of common reporter mice has recently been published to which we refer the interested reader (75).

Procedure

Reporter mice are genetically modified, linking easily measurable "reporter genes" to genes of interest. They are often generated using cre/loxP systems in which certain DNA sequences are flanked by two loxP sites. DNA between these sites will be excised in the presence of activated cre recombinase (which may be linked to other genes to localize its expression to certain cells, tissues, events etc). The net effect of this deletion in reporter mice is often activation of the expression of reporter genes which may encode fluorescent (green fluorescent protein and red fluorescent protein) or non-fluorescent (chloramphenicol acetyltransferase and lacZ) proteins, linked to the expression of genes of interest. Imaging technologies may then be used for a variety of assessments including spatiotemporal gene expression, live cell imaging, lineage tracing, and analysis of cell morphology (76).

Another commonly implemented genetic technique in fracture repair studies is quantitative real time polymerase chain reaction (qRT-PCR). qRT-PCR is a variant of standard PCR, and measures the relative abundance of mRNA of specific genes within a sample. It involves reverse transcribing RNA into DNA followed by several rounds of DNA amplification in the presence of DNA binding fluorescent molecules. This fluorescence is then measured to determine the quantity of amplified DNA which will be directly proportionate to the initial quantity of mRNA (77).

Newer methods of gene expression analyses are also becoming more widely available, including RNA-seq, scRNA-seq and ATAC-seq. RNA-seq and scRNA-seq enable efficient quantification of genome wide expression within a sample or individual cells respectively. In general, RNA sequencing involves isolation and purification of RNA followed by fragmentation and reverse transcription to generate cDNA. Sequencing adapters are then ligated to the ends of these fragments, and they are read by a sequencing platform (78). scRNA involves additional considerations for capturing single cells and unbiased cDNA amplification (79). ATAC-seq works similarly except adapters are ligated to accessible segments of DNA allowing investigators to assess chromatin accessibility (80). There are many sequencing platforms available such as Illumina HiSeq for traditional RNA seq, 10x Genomics Chromium or BD Rhapsody for scRNA seq and Illumina KAPA library quant kit for ATAC-seq.

Outcomes

Potential targets of these investigations in fracture repair studies are vast, including genes related to the extracellular matrix, growth and differentiation factors, matrix metalloproteinases and angiogenic factors (78). Hadjiargyrou *et al* have identified 704 genes of particular significance to the fracture repair process (79). Fracture healing investigations often utilize qRT-PCR, RNA sequencing and reporter mice to study the role of these genes in the molecular and cellular processes of fracture repair (80-85).

Selection, Integration, and Planning of Fracture Repair Assessments

Generally, multiple or all mentioned methodologies are included in fracture repair studies, as they tend to complement one another so that their combined application offers more than the sum of their individual assessments. Examples of this principle are evident in studies examining the impact of bisphosphonate and alcohol administration on fracture repair. Bisphosphonate administration has been shown to concurrently increase mechanical strength and decrease material quality throughout repair, and it was concluded this was due to increased callus volume compensating for decreased quality (86). In these studies, if only mechanical testing had been performed, they may have concluded that bisphosphonates improved fracture repair outcomes, however this is not necessarily the case. Furthermore, a study investigating alcohol administration on fracture repair observed decreased mechanical stiffness despite unchanged tissue volumes, likely as a manifestation of compositional rather than structural aberrancy (42). In this study, if just structural and mechanical assessments had been performed, there would not have been a satisfactory explanation for observed mechanical deficits.

For reasons such as these, in fracture repair studies it is often valuable to include a combination of mechanical, structural and compositional assessments, although method selection will largely vary depending on specific hypotheses being tested. All forms of assessment discussed in this review fit their own niche for investigating fracture repair and together act synergistically, each expanding the significance that may be derived from the rest. Table 2 provides an overview of relevant parameters of each methodology

and Figure 7 offers an approximate timeline for conducting assessments throughout repair process.

Though beyond the scope of this review, statistical analysis is essential in designing experiments and interpreting their results and must be tailored to the hypothesis being tested. This requires careful consideration of the experimental design, procedures for randomization, blinding of investigators, statistical methods, and power of analysis before initiating any experiment, often necessitating the expertise of an experienced statistician (87, 88).

Radiograph

X-rays are the least time intensive method and can be performed *in vivo* without risk of disrupting healing processes (unlike μCT). For these reasons, they are often performed once or twice a week throughout the course of the study, as well as immediately following fracture creation and prior to euthanasia (Figure 7). This method offers a clinically relevant approximation of fracture healing progression, although tends to be limited due to subjectivity and high intra and inter-observer variability (20). RUST and mRUST offer potentially more reliable, consistent approaches to scoring X-rays, with both human and murine studies giving ICC values between 0.63 and 0.86 (17-19), which indicates substantial agreement in assessment (89); however, X-ray still cannot wholly replace μCT and histomorphometry as it is a much lower resolution view of the architecture and cannot adequately assess soft tissue (cartilage and fibrous) (89).

Biomarkers

Biomarkers offer noninvasive and inexpensive means of assessing fracture healing stage and local and systemic processes related to fracture healing. Due to the relative convenience of this methodology, biomarkers are often measured once or twice a week throughout the repair process (26, 28). Beyond their role in tracking fracture repair progress in these studies, many biomarkers may possess direct clinical utility in early identification of non-unions (33-35).

Micro-Computed Tomography

µCT offers the highest resolution visualization of fracture callus architecture and is the only structural assessment to offer precise volumetric measures. It may be conducted *in vivo*, yet this may result in lower resolution and altered repair (39, 40).

Typical µCT is limited in that it cannot distinguish cartilage from fibrous tissue and, prior to callus bridging, has trouble distinguishing any form of soft tissue from the surrounding apparatus (45). For these reasons, it is best suited for analysis of mineralized bone, and therefore is most effectively implemented at and after the expected onset of the hard callus stage of repair, 2-3 weeks post fracture (Figure 7). However, it is non-destructive so it can be completed on bones prior to either histology or mechanical testing (which are both destructive and cannot be conducted on the same bones), regardless of time point.

Histomorphometry

Structural histologic assessments offer the best distinction of tissue types (bone, cartilage, fibrous and marrow) and observation of tissues unseen on radiograph or µCT, particularly during early healing (hematoma, chondrogenic, calcified cartilage phase and early bone formation). The distinction between cartilage and fibrous tissue is of particular importance because fibrous tissue filling the fracture defect may indicate poor ossification, while cartilage indicates the opposite, and excessive fibrous tissue formation is a key sign of non-union (68).

Due to this ability to distinguish soft tissues and non-mineralized tissues, histomorphometric assessments complement typical µCT well (as typical µCT cannot differentiate these) and are generally most usefully employed at and after the anticipated onset of the cartilaginous stage of repair, 1-2 weeks post fracture (Figure 7). One promising alternative to traditional histomorphometric assessment that can measure soft tissue *in vivo* is MRI (90).

Additionally, immunohistochemistry offers the ability to localize expression of proteins of interest at the fracture site. While quantitation is possible, data generated primarily point to the mechanisms underlying bone healing progression.

Biomechanics

Biomechanical tests offer the most direct measures of bone functionality, however, they are limited due to their high degree of variability, especially in bending tests (45). Due to this high variability and the fact that both mechanical testing and histology are

destructive (and therefore cannot both be conducted on the same samples), it is usually best to designate larger portions of each experimental group for biomechanical testing. These tests are usually reserved towards the anticipated end of the repair process, 3 to 4 weeks post fracture (Figure 7).

Gene Expression

Gene expression investigations utilizing qRT-PCR, RNA sequencing and reporter mice elucidate the cellular and molecular processes underlying fracture repair. These approaches may be tailored to any point throughout repair depending on specific hypotheses being tested and are often conducted *ex vivo* requiring fracture callus extraction followed by imaging (reporter mice) or callus tissue homogenization and RNA isolation and purification (qRT-PCR) (76, 79). Both these assessments are destructive so investigators must consider what portion of samples to allocate to these tests rather than histologic or biomechanical tests. This decision will depend on the emphasis of the study and the anticipated intraclass variance in gene expression under investigation (greater variance may necessitate larger sample sizes).

Conclusion

This article presents an overview of quantifying fracture repair outcomes in mice including descriptions of the major methodologies, the interpretation of relevant outcome parameters, and key considerations for tactfully selecting, integrating, and planning these assessments. Thoughtful coordination and synthesis of these approaches is critical for evaluating the efficacy of new fracture healing interventions. Moving forward, more data

must be gathered and assessed to ascertain the validity of new techniques (eg, mRUST, *in vivo* μCT, MRI and biomarkers) and their potential for improving the efficiency, clinical relevance, and capacity for precise evaluation of outcomes in fracture repair investigations. Novel assessment modalities may at some point become surrogates for their more labor intensive and expensive traditional counterparts. Continual reassessment and reconsolidation of investigative approaches will be necessary.

Acknowledgements

This project was funded, in part by the Indiana University School of Medicine (RMN, MAK, CDC), and by T35HL110854 (AMK), T32AR065971 (ACM), and R01AG060621 (MAK)from the National Institutes of Health. This material is also the result of work supported with resources and the use of facilities at the Richard L. Roudebush VA Medical Center, Indianapolis, IN: VA Merit #BX003751.

The content of this manuscript is solely the responsibility of the authors and does not necessarily represent the official views of the aforementioned agencies.

References

1. Ensrud KE. Epidemiology of fracture risk with advancing age. J Gerontol A Biol Sci Med Sci. 2013;68(10):1236-42. Epub 2013/07/09. doi: 10.1093/gerona/glt092. PubMed PMID: 23833201.

2. Burge R, Dawson-Hughes B, Solomon DH, et al. Incidence and economic burden of osteoporosis-related fractures in the United States, 2005-2025. J Bone Miner Res. 2007;22(3):465-75. Epub 2006/12/06. doi: 10.1359/jbmr.061113. PubMed PMID: 17144789.

3. Schnell S, Friedman SM, Mendelson DA, et al. The 1-year mortality of patients treated in a hip fracture program for elders. Geriatr Orthop Surg Rehabil. 2010;1(1):6-14.

Epub 2010/09/01. doi: 10.1177/2151458510378105. PubMed PMID: 23569656; PubMed Central PMCID: PMCPMC3597289.

4. Keating JF, O'Brien PJ, Blachut PA, et al. Locking intramedullary nailing with and without reaming for open fractures of the tibial shaft. A prospective, randomized study. J Bone Joint Surg Am. 1997;79(3):334-41. Epub 1997/03/01. doi: 10.2106/00004623-199703000-00003. PubMed PMID: 9070520.

5. group TIw, Busse JW, Bhandari M, et al. Re-evaluation of low intensity pulsed ultrasound in treatment of tibial fractures (TRUST): randomized clinical trial. BMJ. 2016;355:i5351. Epub 2016/11/01. doi: 10.1136/bmj.i5351. PubMed PMID: 27797787; PubMed Central PMCID: PMCPMC5080447 at www.icmje.org/coi_disclosure.pdf and declare: TAE, ES, and MB have received consulting fees from Smith & Nephew, the manufacturer of the study device. PT receives royalties from Smith & Nephew. GJDR is a paid consultant for Bioventus LLC, which is 51% owned by Essex Woodlands and 49% by Smith & Nephew. MB is supported, in part, by a Canada research chair, McMaster University.

6. Sheen JR, Garla VV. Fracture Healing Overview. StatPearls. Treasure Island (FL)2020.

7. Mizoguchi T, Ono N. The diverse origin of bone-forming osteoblasts. J Bone Miner Res. 2021. Epub 2021/07/03. doi: 10.1002/jbmr.4410. PubMed PMID: 34213032.

8. Wolff LI, Hartmann C. A Second Career for Chondrocytes-Transformation into Osteoblasts. Curr Osteoporos Rep. 2019;17(3):129-37. Epub 2019/04/06. doi: 10.1007/s11914-019-00511-3. PubMed PMID: 30949840.

9. Einhorn TA, Gerstenfeld LC. Fracture healing: mechanisms and interventions. Nat Rev Rheumatol. 2015;11(1):45-54. Epub 2014/10/01. doi: 10.1038/nrrheum.2014.164. PubMed PMID: 25266456; PubMed Central PMCID: PMCPMC4464690.

10. Einhorn TA. The cell and molecular biology of fracture healing. Clin Orthop Relat Res. 1998(355 Suppl):S7-21. Epub 1999/01/26. doi: 10.1097/00003086-199810001-00003. PubMed PMID: 9917622.

11. Marsell R, Einhorn TA. The biology of fracture healing. Injury. 2011;42(6):551-5. Epub 2011/04/15. doi: 10.1016/j.injury.2011.03.031. PubMed PMID: 21489527; PubMed Central PMCID: PMCPMC3105171.

12. Perren SM. Physical and biological aspects of fracture healing with special reference to internal fixation. Clin Orthop Relat Res. 1979(138):175-96. Epub 1979/01/01. PubMed PMID: 376198.

13. Marsell R, Einhorn TA. Emerging bone healing therapies. J Orthop Trauma. 2010;24 Suppl 1:S4-8. Epub 2010/03/10. doi: 10.1097/BOT.0b013e3181ca3fab. PubMed PMID: 20182234.

14. Histing T, Marciniak K, Scheuer C, et al. Sildenafil accelerates fracture healing in mice. J Orthop Res. 2011;29(6):867-73. Epub 2011/01/20. doi: 10.1002/jor.21324. PubMed PMID: 21246617.

15. Collier CD, Hausman BS, Zulqadar SH, et al. Characterization of a reproducible model of fracture healing in mice using an open femoral osteotomy. Bone Rep. 2020;12:100250. Epub 2020/02/25. doi: 10.1016/j.bonr.2020.100250. PubMed PMID: 32090156; PubMed Central PMCID: PMCPMC7025178.

16. Li S, Xiang C, Wei X, et al. Knockdown Indian Hedgehog (Ihh) does not delay Fibular Fracture Healing in genetic deleted Ihh mice and pharmaceutical inhibited Ihh Mice. Sci Rep. 2018;8(1):10351. Epub 2018/07/10. doi: 10.1038/s41598-018-28657-7. PubMed PMID: 29985470; PubMed Central PMCID: PMCPMC6037729.

17. Litrenta J, Tornetta P, 3rd, Mehta S, et al. Determination of Radiographic Healing: An Assessment of Consistency Using RUST and Modified RUST in Metadiaphyseal Fractures. J Orthop Trauma. 2015;29(11):516-20. Epub 2015/07/15. doi: 10.1097/BOT.0000000000000390. PubMed PMID: 26165265.

18. Kooistra BW, Dijkman BG, Busse JW, et al. The radiographic union scale in tibial fractures: reliability and validity. J Orthop Trauma. 2010;24 Suppl 1:S81-6. Epub 2010/03/10. doi: 10.1097/BOT.0b013e3181ca3fd1. PubMed PMID: 20182243.

19. Cooke ME, Hussein AI, Lybrand KE, et al. Correlation between RUST assessments of fracture healing to structural and biomechanical properties. J Orthop Res. 2018;36(3):945-53. Epub 2017/08/24. doi: 10.1002/jor.23710. PubMed PMID: 28833572; PubMed Central PMCID: PMCPMC5823715.

20. Corrales LA, Morshed S, Bhandari M, Miclau T, 3rd. Variability in the assessment of fracture-healing in orthopaedic trauma studies. J Bone Joint Surg Am. 2008;90(9):1862-8. Epub 2008/09/03. doi: 10.2106/JBJS.G.01580. PubMed PMID: 18762645; PubMed Central PMCID: PMCPMC2663323.

21. Morgan EF, Mason ZD, Chien KB, et al. Micro-computed tomography assessment of fracture healing: relationships among callus structure, composition, and mechanical function. Bone. 2009;44(2):335-44. Epub 2008/11/18. doi: 10.1016/j.bone.2008.10.039. PubMed PMID: 19013264; PubMed Central PMCID: PMCPMC2669651.

22. Jamsa T, Koivukangas A, Kippo K, et al. Comparison of radiographic and pQCT analyses of healing rat tibial fractures. Calcif Tissue Int. 2000;66(4):288-91. Epub 2000/04/01. doi: 10.1007/s002230010058. PubMed PMID: 10742447.

23. Panjabi MM, Walter SD, Karuda M, et al. Correlations of radiographic analysis of healing fractures with strength: a statistical analysis of experimental osteotomies. J Orthop Res. 1985;3(2):212-8. Epub 1985/01/01. doi: 10.1002/jor.1100030211. PubMed PMID: 3998898.

24. Whelan DB, Bhandari M, Stephen D, et al. Development of the radiographic union score for tibial fractures for the assessment of tibial fracture healing after intramedullary fixation. J Trauma. 2010;68(3):629-32. Epub 2009/12/10. doi: 10.1097/TA.0b013e3181a7c16d. PubMed PMID: 19996801.

25. Litrenta J, Tornetta P, 3rd, Ricci W, et al. In Vivo Correlation of Radiographic Scoring (Radiographic Union Scale for Tibia Fractures) and Biomechanical Data in a Sheep Osteotomy Model: Can We Define Union Radiographically? J Orthop Trauma. 2017;31(3):127-30. Epub 2017/01/11. doi: 10.1097/BOT.0000000000000753. PubMed PMID: 28072652.

26. Cook GE, Bates BD, Tornetta P, et al. Assessment of Fracture Repair. J Orthop Trauma. 2015;29 Suppl 12:S57-61. Epub 2015/11/20. doi: 10.1097/BOT.0000000000000470. PubMed PMID: 26584269.

27. Cox KL, Devanarayan V, Kriauciunas A, et al. Immunoassay Methods. In: Markossian S, Sittampalam GS, Grossman A, Brimacombe K, Arkin M, Auld D, et al., editors. Assay Guidance Manual. Bethesda (MD)2004.

28. Hussein AI, Mancini C, Lybrand KE, et al. Serum proteomic assessment of the progression of fracture healing. J Orthop Res. 2018;36(4):1153-63. Epub 2017/10/04. doi: 10.1002/jor.23754. PubMed PMID: 28971515; PubMed Central PMCID: PMCPMC5880751.

29. Dohke T, Iba K, Hanaka M, et al. Teriparatide rapidly improves pain-like behavior in ovariectomized mice in association with the downregulation of inflammatory cytokine expression. J Bone Miner Metab. 2018;36(5):499-507. Epub 2017/10/07. doi: 10.1007/s00774-017-0865-0. PubMed PMID: 28983699.

30. Hojsager FD, Rand MS, Pedersen SB, et al. Fracture-induced changes in biomarkers CTX, PINP, OC, and BAP-a systematic review. Osteoporos Int. 2019;30(12):2381-9. Epub 2019/08/26. doi: 10.1007/s00198-019-05132-1. PubMed PMID: 31446441.

31. Working ZM, Morris ER, Chang JC, et al. A quantitative serum biomarker of circulating collagen X effectively correlates with endochondral fracture healing. J Orthop Res. 2021;39(1):53-62. Epub 2020/06/14. doi: 10.1002/jor.24776. PubMed PMID: 32533783.

32. Gao F, Lv TR, Zhou JC, Qin XD. Effects of obesity on the healing of bone fracture in mice. J Orthop Surg Res. 2018;13(1):145. Epub 2018/06/09. doi:

10.1186/s13018-018-0837-7. PubMed PMID: 29880016; PubMed Central PMCID: PMCPMC5992669.

33. Hankenson KD, Zimmerman G, Marcucio R. Biological perspectives of delayed fracture healing. Injury. 2014;45 Suppl 2:S8-S15. Epub 2014/05/27. doi: 10.1016/j.injury.2014.04.003. PubMed PMID: 24857030; PubMed Central PMCID: PMCPMC4406220.

34. Albeshri S, Alblaihess A, Niazy AA, et al. Biomarkers as Independent Predictors of Bone Regeneration around Biomaterials: A Systematic Review of Literature. J Contemp Dent Pract. 2018;19(5):605-18. Epub 2018/05/29. PubMed PMID: 29807974.

35. Pountos I, Georgouli T, Pneumaticos S, Giannoudis PV. Fracture non-union: Can biomarkers predict outcome? Injury. 2013;44(12):1725-32. Epub 2013/10/01. doi: 10.1016/j.injury.2013.09.009. PubMed PMID: 24075219.

36. Vesper EO, Hammond MA, Allen MR, Wallace JM. Even with rehydration, preservation in ethanol influences the mechanical properties of bone and how bone responds to experimental manipulation. Bone. 2017;97:49-53. Epub 2017/01/07. doi: 10.1016/j.bone.2017.01.001. PubMed PMID: 28057526; PubMed Central PMCID: PMCPMC5367983.

37. Tiefenboeck TM, Payr S, Bajenov O, et al. Author Correction: Effect of two (short-term) storage methods on load to failure testing of murine bone tissue. Sci Rep. 2020;10(1):9983. Epub 2020/06/18. doi: 10.1038/s41598-020-66764-6. PubMed PMID: 32546708; PubMed Central PMCID: PMCPMC7298020.

38. Campbell GM, Sophocleous A. Quantitative analysis of bone and soft tissue by micro-computed tomography: applications to ex vivo and in vivo studies. Bonekey Rep. 2014;3:564. Epub 2014/09/04. doi: 10.1038/bonekey.2014.59. PubMed PMID: 25184037; PubMed Central PMCID: PMCPMC4140449.

39. Willekens I, Buls N, Lahoutte T, et al. Evaluation of the radiation dose in micro-CT with optimization of the scan protocol. Contrast Media Mol Imaging. 2010;5(4):201-7. Epub 2010/07/29. doi: 10.1002/cmmi.394. PubMed PMID: 20665903.

40. Klinck RJ, Campbell GM, Boyd SK. Radiation effects on bone architecture in mice and rats resulting from in vivo micro-computed tomography scanning. Med Eng Phys. 2008;30(7):888-95. Epub 2008/02/06. doi: 10.1016/j.medengphy.2007.11.004. PubMed PMID: 18249025.

41. Bouxsein ML, Boyd SK, Christiansen BA, et al. Guidelines for assessment of bone microstructure in rodents using micro-computed tomography. J Bone Miner Res. 2010;25(7):1468-86. Epub 2010/06/10. doi: 10.1002/jbmr.141. PubMed PMID: 20533309.

42. Natoli RM, Yu H, Meislin MC, et al. Alcohol exposure decreases osteopontin expression during fracture healing and osteopontin-mediated mesenchymal stem cell migration in vitro. J Orthop Surg Res. 2018;13(1):101. Epub 2018/04/28. doi: 10.1186/s13018-018-0800-7. PubMed PMID: 29699560; PubMed Central PMCID: PMCPMC5921778.

43. Childress P, Brinker A, Gong CS, et al. Forces associated with launch into space do not impact bone fracture healing. Life Sci Space Res (Amst). 2018;16:52-62. Epub 2018/02/25. doi: 10.1016/j.lssr.2017.11.002. PubMed PMID: 29475520; PubMed Central PMCID: PMCPMC5828031.

44. Gardner MJ, van der Meulen MC, Demetrakopoulos D, et al. In vivo cyclic axial compression affects bone healing in the mouse tibia. J Orthop Res. 2006;24(8):1679-86. Epub 2006/06/22. doi: 10.1002/jor.20230. PubMed PMID: 16788988; PubMed Central PMCID: PMCPMC2944415.

45. O'Neill KR, Stutz CM, Mignemi NA, et al. Micro-computed tomography assessment of the progression of fracture healing in mice. Bone. 2012;50(6):1357-67. Epub 2012/03/29. doi: 10.1016/j.bone.2012.03.008. PubMed PMID: 22453081.

46. Cengiz IF, Oliveira JM, Reis RL. Micro-computed tomography characterization of tissue engineering scaffolds: effects of pixel size and rotation step. J Mater Sci Mater Med. 2017;28(8):129. Epub 2017/07/20. doi: 10.1007/s10856-017-5942-3. PubMed PMID: 28721665.

47. Cole J, van der Meulen M. Biomechanics of Bone. 2010. p. 157-79.

48. Taiani JT, Buie HR, Campbell GM, et al. Embryonic stem cell therapy improves bone quality in a model of impaired fracture healing in the mouse; tracked temporally using in vivo micro-CT. Bone. 2014;64:263-72. Epub 2014/05/02. doi: 10.1016/j.bone.2014.04.019. PubMed PMID: 24780879.

49. Liao MH, Lin PI, Ho WP, et al. Participation of GATA-3 in regulation of bone healing through transcriptional upregulation of bcl-xL expression. Exp Mol Med. 2017;49(11):e398. Epub 2017/11/25. doi: 10.1038/emm.2017.182. PubMed PMID: 29170477; PubMed Central PMCID: PMCPMC5704189.

50. Mehta M, Heyland M, Toben D, Duda GN. Microstructure and homogeneity of distribution of mineralised struts determine callus strength. Eur Cell Mater. 2013;25:366-79; discussion 78-9. Epub 2013/07/09. doi: 10.22203/ecm.v025a26. PubMed PMID: 23832689.

51. Ai-Aql ZS, Alagl AS, Graves DT, et al. Molecular mechanisms controlling bone formation during fracture healing and distraction osteogenesis. J Dent Res. 2008;87(2):107-18. Epub 2008/01/26. doi: 10.1177/154405910808700215. PubMed PMID: 18218835; PubMed Central PMCID: PMCPMC3109437.

52. Donnelly E. Methods for assessing bone quality: a review. Clin Orthop Relat Res. 2011;469(8):2128-38. Epub 2010/12/01. doi: 10.1007/s11999-010-1702-0. PubMed PMID: 21116752; PubMed Central PMCID: PMCPMC3126959.

53. Lu C, Marcucio R, Miclau T. Assessing angiogenesis during fracture healing. Iowa Orthop J. 2006;26:17-26. Epub 2006/06/23. PubMed PMID: 16789443; PubMed Central PMCID: PMCPMC1888583.

54. Hayward LN, de Bakker CM, Lusic H, et al. MRT letter: Contrast-enhanced computed tomographic imaging of soft callus formation in fracture healing. Microsc Res Tech. 2012;75(1):7-14. Epub 2011/11/01. doi: 10.1002/jemt.21100. PubMed PMID: 22038692; PubMed Central PMCID: PMCPMC3380422.

55. Zhang G, Wang S, Xu S, et al. The Effect of Formalin Preservation Time and Temperature on the Material Properties of Bovine Femoral Cortical Bone Tissue. Ann Biomed Eng. 2019;47(4):937-52. Epub 2019/01/24. doi: 10.1007/s10439-019-02197-1. PubMed PMID: 30671755.

56. Buesa RJ. Histology without formalin? Ann Diagn Pathol. 2008;12(6):387-96. Epub 2008/11/11. doi: 10.1016/j.anndiagpath.2008.07.004. PubMed PMID: 18995201.

57. *RJ B*. Histology without formalin? Ann diagn Pathol. 2008. PubMed Central PMCID: PMC18995201.

58. Kacena MA, Troiano NW, Coady CE, Horowitz MC. HistoChoice as an alternative to formalin fixation of undecalcified bone specimens. Biotech Histochem. 2004;79(5-6):185-90. Epub 2005/03/15. doi: 10.1080/10520290400015506. PubMed PMID: 15764285.

59. Liu H, Zhu R, Liu C, et al. Evaluation of Decalcification Techniques for Rat Femurs Using HE and Immunohistochemical Staining. Biomed Res Int. 2017;2017:9050754. Epub 2017/03/02. doi: 10.1155/2017/9050754. PubMed PMID: 28246608; PubMed Central PMCID: PMCPMC5299168 paper.

60. Serowoky MA, Patel DD, Hsieh JW, Mariani FV. The use of commercially available adhesive tapes to preserve cartilage and bone tissue integrity during cryosectioning. Biotechniques. 2018;65(4):191-6. Epub 2018/10/05. doi: 10.2144/btn-2018-0021. PubMed PMID: 30284932; PubMed Central PMCID: PMCPMC6642614.

61. Bhatti FUR, Dadwal UC, Valuch CR, et al. The effects of high fat diet, bone healing, and BMP-2 treatment on endothelial cell growth and function. Bone. 2021;146:115883. Epub 2021/02/14. doi: 10.1016/j.bone.2021.115883. PubMed PMID: 33581374; PubMed Central PMCID: PMCPMC8009863.

62. Egan KP, Brennan TA, Pignolo RJ. Bone histomorphometry using free and commonly available software. 2012;61(6):1168-73. doi: 10.1111/j.1365-2559.2012.04333.x.

63. Taylor CR, Levenson RM. Quantification of immunohistochemistry--issues concerning methods, utility and semiquantitative assessment II. Histopathology. 2006;49(4):411-24. Epub 2006/09/19. doi: 10.1111/j.1365-2559.2006.02513.x. PubMed PMID: 16978205.

64. Muller R, Van Campenhout H, Van Damme B, et al. Morphometric analysis of human bone biopsies: a quantitative structural comparison of histological sections and micro-computed tomography. Bone. 1998;23(1):59-66. Epub 1998/07/14. doi: 10.1016/s8756-3282(98)00068-4. PubMed PMID: 9662131.

65. Cullinane D, Einhorn T. Biomechanics of Bone. 12002. p. 17-32.

66. Gerstenfeld LC, Wronski TJ, Hollinger JO, Einhorn TA. Application of histomorphometric methods to the study of bone repair. J Bone Miner Res. 2005;20(10):1715-22. Epub 2005/09/15. doi: 10.1359/JBMR.050702. PubMed PMID: 16160729.

67. Augat P, Merk J, Genant HK, Claes L. Quantitative assessment of experimental fracture repair by peripheral computed tomography. Calcif Tissue Int. 1997;60(2):194-9. Epub 1997/02/01. doi: 10.1007/s002239900213. PubMed PMID: 9056170.

68. Han Z, Bhavsar M, Leppik L, et al. Histological Scoring Method to Assess Bone Healing in Critical Size Bone Defect Models. Tissue Eng Part C Methods. 2018;24(5):272-9. Epub 2018/02/23. doi: 10.1089/ten.TEC.2017.0497. PubMed PMID: 29466929.

69. Liu A, Li Y, Wang Y, et al. Exogenous Parathyroid Hormone-Related Peptide Promotes Fracture Healing in Lepr(-/-) Mice. Calcif Tissue Int. 2015;97(6):581-91. Epub 2015/09/01. doi: 10.1007/s00223-015-0041-2. PubMed PMID: 26314884.

70. Meganck JA, Begun DL, McElderry JD, et al. Fracture healing with alendronate treatment in the Brtl/+ mouse model of osteogenesis imperfecta. Bone. 2013;56(1):204-12. Epub 2013/06/19. doi: 10.1016/j.bone.2013.06.003. PubMed PMID: 23774443; PubMed Central PMCID: PMCPMC3999166.

71. Sharir A, Barak MM, Shahar R. Whole bone mechanics and mechanical testing. Vet J. 2008;177(1):8-17. Epub 2007/11/08. doi: 10.1016/j.tvjl.2007.09.012. PubMed PMID: 17986396.

72. Steiner M, Volkheimer D, Meyers N, et al. Comparison between different methods for biomechanical assessment of ex vivo fracture callus stiffness in small animal bone healing studies. PLoS One. 2015;10(3):e0119603. Epub 2015/03/18. doi:

10.1371/journal.pone.0119603. PubMed PMID: 25781027; PubMed Central PMCID: PMCPMC4363594.

73. Boccaccio A, Ballini A, Pappalettere C, et al. Finite element method (FEM), mechanobiology and biomimetic scaffolds in bone tissue engineering. Int J Biol Sci. 2011;7(1):112-32. Epub 2011/02/01. doi: 10.7150/ijbs.7.112. PubMed PMID: 21278921; PubMed Central PMCID: PMCPMC3030147.

74. Frei H, Mitchell P, Masri BA, et al. Mechanical characteristics of the bone-graft-cement interface after impaction allografting. J Orthop Res. 2005;23(1):9-17. Epub 2004/12/21. doi: 10.1016/j.orthres.2004.05.012. PubMed PMID: 15607869.

75. Bahney CS, Zondervan RL, Allison P, et al. Cellular biology of fracture healing. J Orthop Res. 2019;37(1):35-50. Epub 2018/10/30. doi: 10.1002/jor.24170. PubMed PMID: 30370699; PubMed Central PMCID: PMCPMC6542569.

76. Li S, Chen LX, Peng XH, et al. Overview of the reporter genes and reporter mouse models. Animal Model Exp Med. 2018;1(1):29-35. Epub 2019/03/21. doi: 10.1002/ame2.12008. PubMed PMID: 30891544; PubMed Central PMCID: PMCPMC6357428.

77. Ginzinger DG. Gene quantification using real-time quantitative PCR: an emerging technology hits the mainstream. Exp Hematol. 2002;30(6):503-12. Epub 2002/06/14. doi: 10.1016/s0301-472x(02)00806-8. PubMed PMID: 12063017.

78. Dimitriou R, Giannoudis PV. The genetic profile of bone repair. Clin Cases Miner Bone Metab. 2013;10(1):19-21. Epub 2013/07/17. doi: 10.11138/ccmbm/2013.10.1.019. PubMed PMID: 23858305; PubMed Central PMCID: PMCPMC3710004.

79. Hadjiargyrou M, Lombardo F, Zhao S, et al. Transcriptional profiling of bone regeneration. Insight into the molecular complexity of wound repair. J Biol Chem. 2002;277(33):30177-82. Epub 2002/06/11. doi: 10.1074/jbc.M203171200. PubMed PMID: 12055193.

80. Cui Y, Fu S, Sun D, et al. EPC-derived exosomes promote osteoclastogenesis through LncRNA-MALAT1. J Cell Mol Med. 2019;23(6):3843-54. Epub 2019/04/27. doi: 10.1111/jcmm.14228. PubMed PMID: 31025509; PubMed Central PMCID: PMCPMC6533478.

81. Xie Y, Luo F, Xu W, et al. FGFR3 deficient mice have accelerated fracture repair. Int J Biol Sci. 2017;13(8):1029-37. Epub 2017/09/20. doi: 10.7150/ijbs.19309. PubMed PMID: 28924384; PubMed Central PMCID: PMCPMC5599908.

82. Ushiku C, Adams DJ, Jiang X, et al. Long bone fracture repair in mice harboring GFP reporters for cells within the osteoblastic lineage. J Orthop Res. 2010;28(10):1338-47. Epub 2010/09/15. doi: 10.1002/jor.21105. PubMed PMID: 20839319.

83. Li Z, Meyers CA, Chang L, et al. Fracture repair requires TrkA signaling by skeletal sensory nerves. J Clin Invest. 2019;129(12):5137-50. Epub 2019/10/23. doi: 10.1172/JCI128428. PubMed PMID: 31638597; PubMed Central PMCID: PMCPMC6877307.

84. Coates BA, McKenzie JA, Buettmann EG, et al. Transcriptional profiling of intramembranous and endochondral ossification after fracture in mice. Bone. 2019;127:577-91. Epub 2019/08/02. doi: 10.1016/j.bone.2019.07.022. PubMed PMID: 31369916; PubMed Central PMCID: PMCPMC6708791.

85. Chakraborty N, Waning DL, Gautam A, et al. Gene-Metabolite Network Linked to Inhibited Bioenergetics in Association With Spaceflight-Induced Loss of Male Mouse Quadriceps Muscle. J Bone Miner Res. 2020;35(10):2049-57. Epub 2020/06/09. doi: 10.1002/jbmr.4102. PubMed PMID: 32511780; PubMed Central PMCID: PMCPMC7689867.

86. Sloan AV, Martin JR, Li S, Li J. Parathyroid hormone and bisphosphonate have opposite effects on stress fracture repair. Bone. 2010;47(2):235-40. Epub 2010/06/29. doi: 10.1016/j.bone.2010.05.015. PubMed PMID: 20580684.

87. Festing MF. Design and statistical methods in studies using animal models of development. ILAR J. 2006;47(1):5-14. Epub 2006/01/05. doi: 10.1093/ilar.47.1.5. PubMed PMID: 16391426.

88. Choi KR, Ryu JY, Lee SY. Revisiting Statistical Design and Analysis in Scientific Research. Small. 2018;14(40):e1802604. Epub 2018/09/27. doi: 10.1002/smll.201802604. PubMed PMID: 30256531.

89. Landis JR, Koch GG. The measurement of observer agreement for categorical data. Biometrics. 1977;33(1):159-74. Epub 1977/03/01. PubMed PMID: 843571.

90. Taha MA, Manske SL, Kristensen E, et al. Assessment of the efficacy of MRI for detection of changes in bone morphology in a mouse model of bone injury. J Magn Reson Imaging. 2013;38(1):231-7. Epub 2012/11/06. doi: 10.1002/jmri.23876. PubMed PMID: 23125100.

Figures

Figure 1. Example of radiographic imaging of fracture site from both lateral and anteroposterior views. These two perspectives enable evaluation of callus formation and fracture line at “four cortices” of bone. The cropped images represent longitudinal assessment of fracture healing.

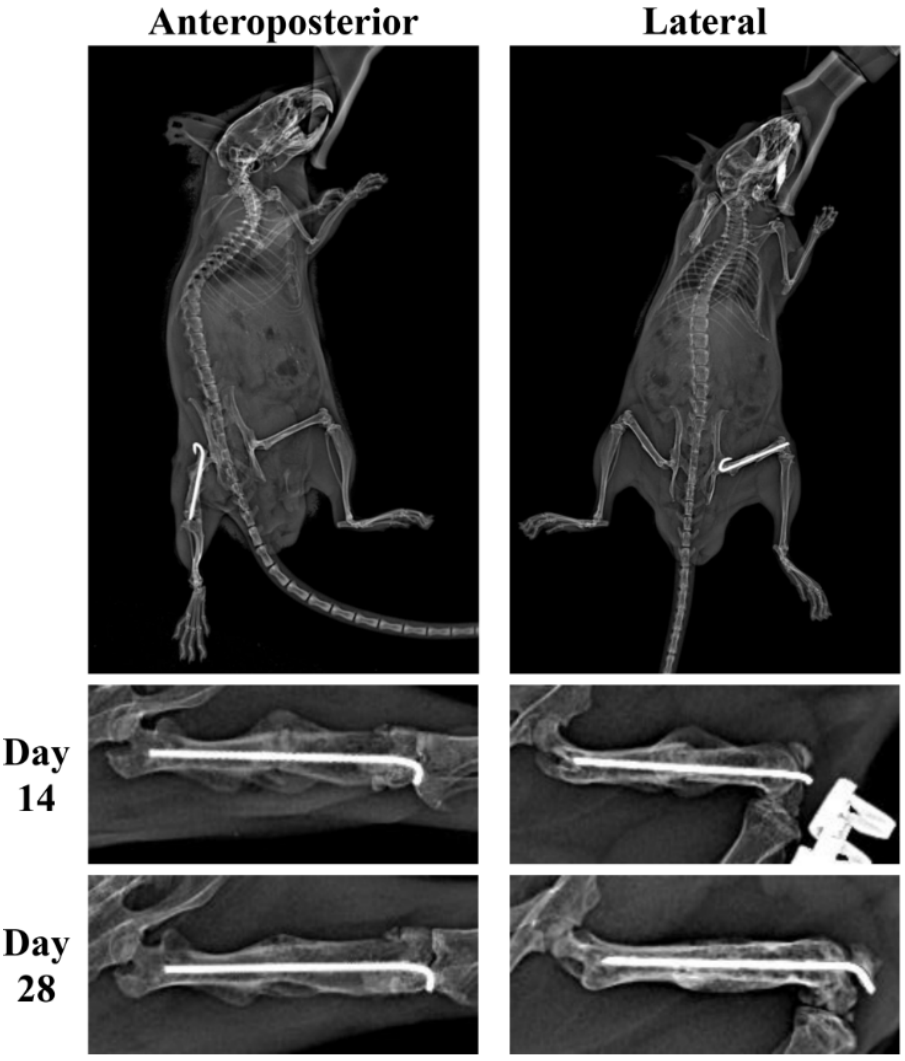

Figure 2. Overview of initial steps to generating volume of interest (VOI). Shadow projection image of fractured femur (A). Fracture midline (B ii.) determined by calculating the midpoint between the first intact cortical ring, proximally (B i.) and distally (B iii.) from the fracture. Complete VOI designated 3.5mm above and below fracture line (C-D). Reprinted with permission from Collier *et al* (15).

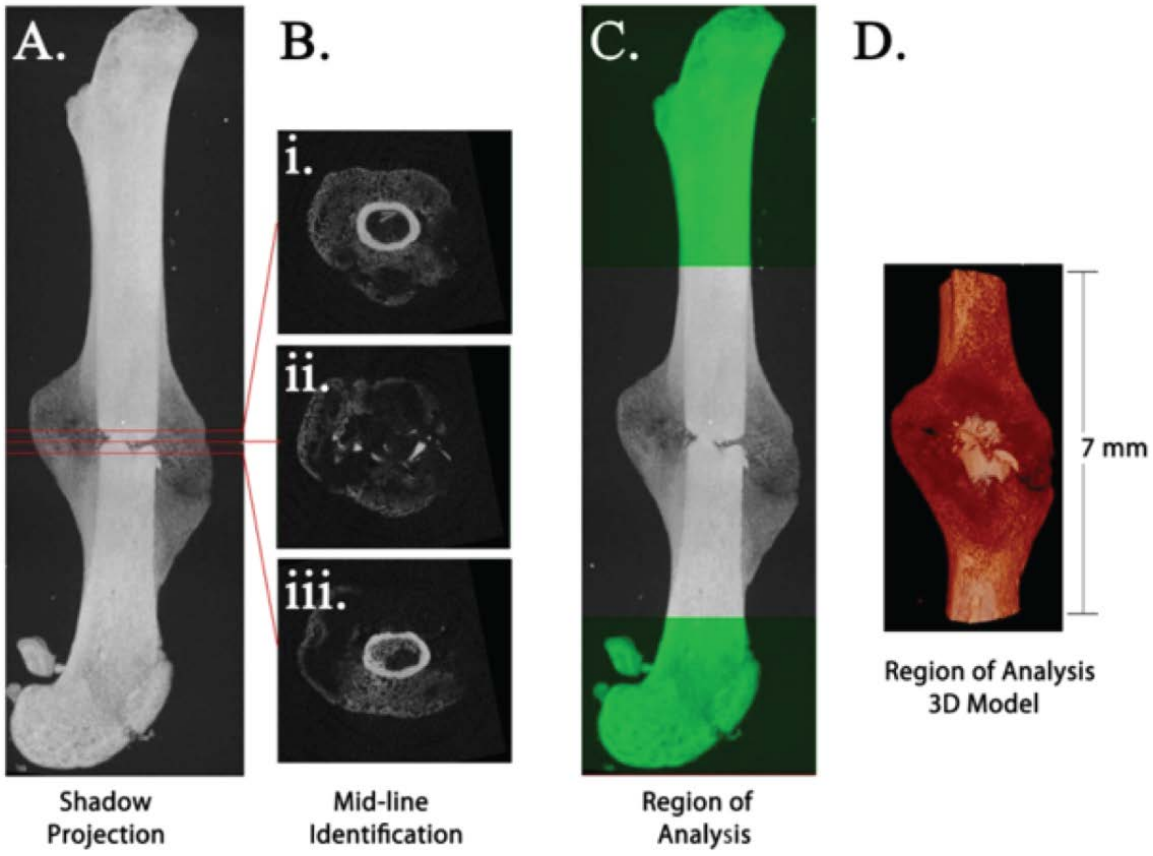

Figure 3. Overview of binarization and final steps of volume of interest (VOI) selection. Example transverse slices through fracture center after binarization (A) and final VOI selection (B) yielding final mineralized callus model (C-D) for morphometric 3D analysis. Reprinted with permission from Collier *et al* (15).

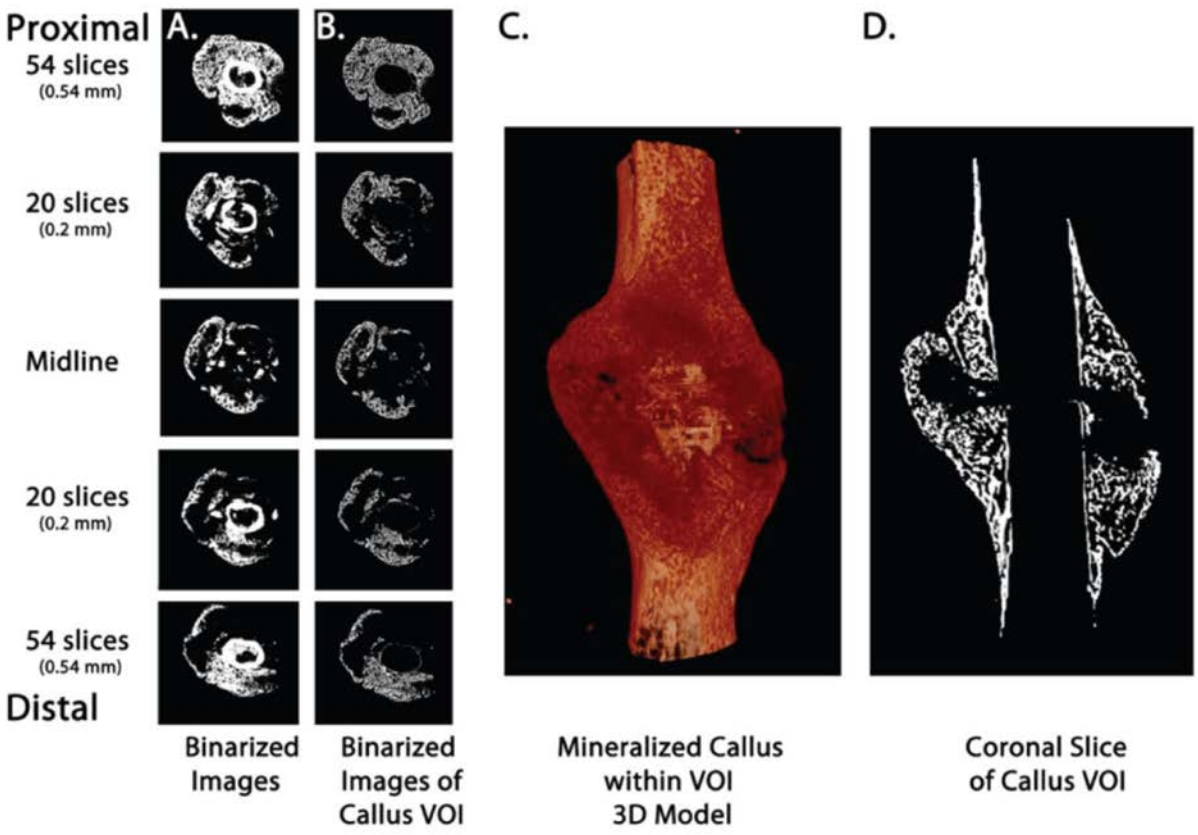

Figure 4. Representative histologic sections stained with picrosirius red (bone) and alcian blue (cartilage) ready for image processing software analysis. Many alternative histologic staining protocols are available for histomorphometric assessment. Adapted with permission from Collier *et al* (15).

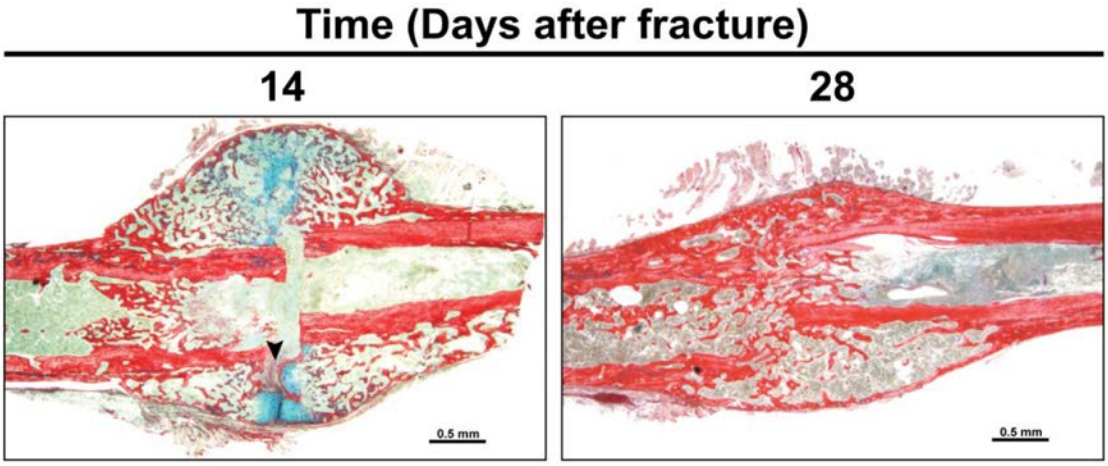

Figure 5. Schematics for biomechanical testing: (A) Three-point bending, (B) Four-point bending, and (C) Torsion testing.

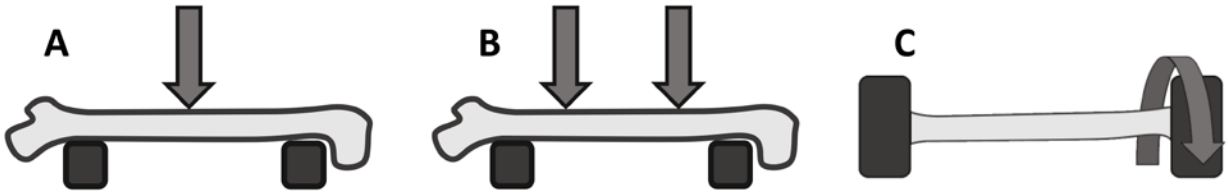

Figure 6. Example torque-angular displacement curve generated from torsional testing. Outcome measures include ultimate torque (torque to fracture point), torsional stiffness (relationship between torque and angular displacement prior to the yield point), twist to failure (angular displacement to fracture point) and toughness (total energy to fracture point; area under torque-angular displacement curve).

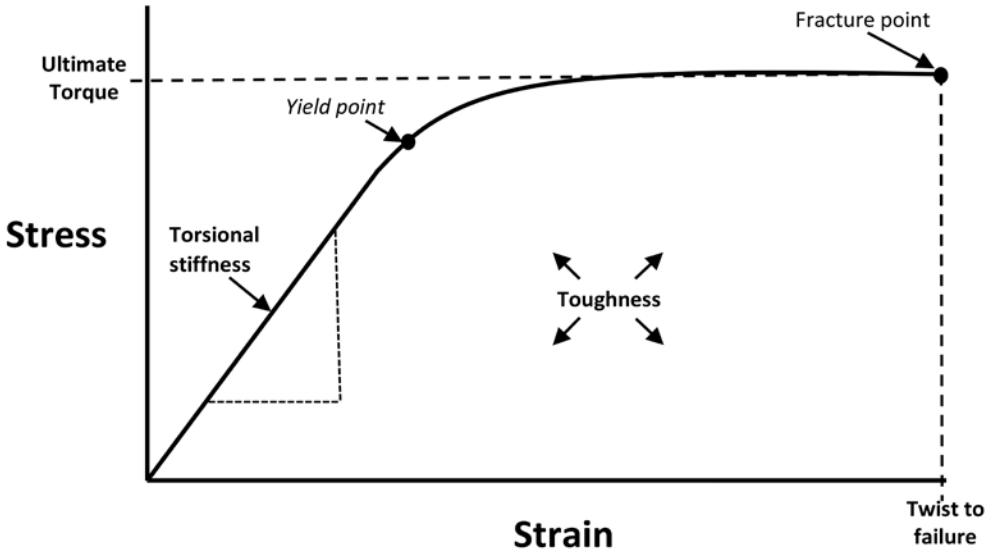

Figure 7. Overview of approximate fracture healing progression and corresponding assessments from 0 to 28 days post fracture.

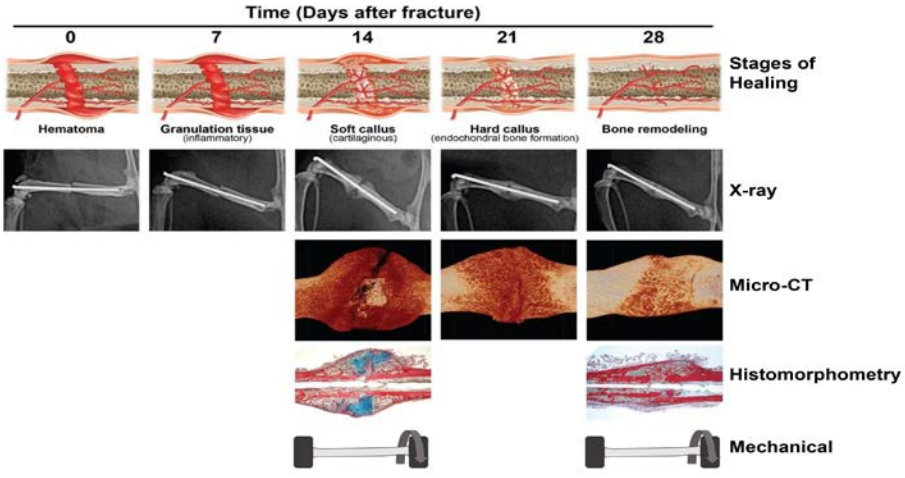

Table 1. RUST and mRUST Scoring Criteria

	Radiographic Criteria		
	Callus	**Fracture Line**	**Score***
RUST	Absent	Visible	1
	Present	Visible	2
	Present	Invisible	3
mRUST	Absent	Visible	1
	Present	Visible	2
	Bridging	Visible	3
	Remodeled	Invisible	4

*A score is given to each of 4 of the orthogonal cortices as viewed from anteroposterior and lateral radiographs. These values are summed together to give a final standard and modified radiographic union scale in tibia (RUST and mRUST, respectively) score.

Table 2. Overview of fracture healing parameters

Radiograph	Units
Callus size	μm^2
Cortical continuity	-
Micro-Computed Tomography	
Tissue volume (TV)	mm^3
Tissue Mineral Density (TMD)	mg HA / cm^3
Bone volume (BV)	mm^3
Bone volume fraction (BV/TV)	%
Bone mineral density (BMD)	mg HA / cm^3
Polar moment of inertia (pMOI)	m^4
Histomorphometry	
Osseous area (OAr)	mm^2
Cartilage area (CgAr)	mm^2
Fibrous area (FbAr)	mm^2
Total callus area (CAr)	mm^2

Void area (VAr)	mm^2
Biomechanics (Torsion)	
Ultimate Torque	N
Torsional stiffness	N/deg
Twist to failure	deg
Toughness	N*deg
Biomechanics (Bending)	
Ultimate force	N
Stiffness	N/mm
Strain	-
Toughness	N*mm

Table 3. Common Histological and Immunohistochemical stains in bone

Stain	Use
Hematoxylin and Eosin	Acidophilic/Basophilic
Collagen Stains	
Picrosirius Red	Collagen
Herovici	Young vs. Mature Collagen
Collagen I, II, X	Collagen types
Cartilage Stains	
Alcian Blue	Proteoglycans in cartilage
Safranin O	Cartilage
Mineralized Bone Stains	
Von Kossa	Calcium/Potassium Mineralization
Alizarin Red	Calcium mineralization
Osteocalcin	Bone matrix synthesis
Differential Stains	
Gömöri Trichrome	Muscle Fibers, Collagen, Nuclei

Hall Brundts Quadruple	Cartilage and Mineralized Bone
Osteoclast Stains	
Tartrate-resistant acid phosphatase (TRAP)	Osteoclast activity
Endothelium	
Endomucin	Angiogenesis
Other	
Osteopontin	Multiple